Inorganic Chemistry

Article

pubs.acs.org/IC

Infrared Spectra of H_2ThS and H_2US in Noble Gas Matrixes: Enhanced H-An-S Covalent Bonding

Xuefeng Wang,[†,‡] Lester Andrews,*[,‡] K. Sahan Thanthiriwatte,[§] and David A. Dixon*[,§]

[†]Department of Chemistry, Tongji University, Shanghai 200092, China
[‡]Department of Chemistry, University of Virginia, P.O. Box 400319, Charlottesville, Virginia 22904-4319, United States
[§]Department of Chemistry, The University of Alabama, Tuscaloosa, Alabama 35487-0336, United States

Supporting Information

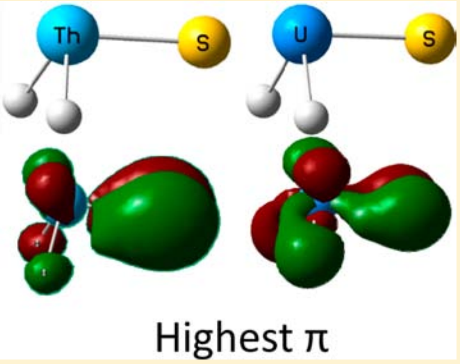

ABSTRACT: Laser-ablated thorium and uranium atoms have been co-deposited at 4 K with hydrogen sulfide in excess noble gas matrixes. The major dihydride sulfide reaction products were observed for each actinide and identified on the basis of S-34 and D isotopic substitution. These assignments were confirmed by frequency and structure calculations using density functional theory with the B3LYP and PW91 exchange-correlation functionals and the CCSD(T) method for the pyramidal H_2ThS ($^1A'$) and H_2US ($^3A''$) molecules. The lowest three spin states of triplet H_2US are calculated to be within 3 kcal/mol using all three methods, just as in H_2UO. The major products are compared with the oxygen analogues H_2ThO and H_2UO, and the sulfides have 71−85 cm^{-1} *higher* hydrogen-actinide stretching frequencies. The actinide-hydrogen bonding appears to be enhanced in the actinide sulfides through back-bonding of a S 3p electron pair to a vacant 6d orbital, which is delocalized over the H atoms. This unique covalent bond is favored by the inductive effect of the hydride substituents, the pyramidal structures, and the lower electronegativity of sulfur. Sulfur back-bonding gives polarized triple bond character to the US and ThS bonds and enhanced metal hydride bonding in H_2ThS and H_2US.

INTRODUCTION

Uranium and thorium bearing species and their reactions with water have been investigated extensively although there has been little study of their reactions with hydrogen sulfide,[1,2] Numerous intermediate hydride, oxide actinide species have been characterized by matrix isolation investigations of their reactions with water and hydrogen peroxide.[3−6] The actinide metal sulfides are refractory materials in their bulk MS, MS_2, and M_2S_3 stoichiometries.[7] The molecular species US, US_2, US_3, ThS, and ThS_2 have been identified in matrix isolation studies from reactions of the laser ablated metals with elemental sulfur vapors, and these identifications have been supported by density functional calculations.[8−10] Two sulfide oxides, SUO and SUO_2, have been investigated using similar methods.[10,11] The nature of the interaction between the actinides in the formal +2, +4, or +6 oxidation states and the O or S atoms has been investigated.[12]

Organoactinides with terminal oxide and sulfide ligands are important for their electronic structure and many applications. The structure and reactivity of oxo and sulfido metallocenes of thorium have been investigated recently, and a complete family of terminal uranium(IV) chalcogenide complexes has been similarly studied.[13] A recent mass spectroscopic and density functional theory (DFT) investigation of diatomic actinide sulfide species concludes that the 5f electrons do not play a substantial role in actinide-sulfur bonding.[14] Coordinating ligands, which potentially involve sulfur as a donor, may have applications in actinide separation processes.[15] Although transition metal hydrides retain their importance in coordination chemistry, there is very little work on actinide metal hydrides owing in part to their reactivity.[16,17]

In the current study, a combined experimental and theoretical investigation of the reactions of laser-ablated thorium and uranium atoms with hydrogen sulfide in excess argon and neon matrixes reveals that H_2ThS and H_2US are the major products formed. The results are compared to the analogous hydride oxide species investigated previously.[3,4] These unusual actinide bearing molecules exhibit characteristics of both hydrides and chalcogenides. It appears that back-donation from the sulfur 3p orbitals to empty 6d orbitals on the actinide plays an important role in the properties of H_2ThS and H_2US where the hydrogen substituents facilitate this process and enhance the metal hydride bonding.

EXPERIMENTAL AND COMPUTATIONAL METHODS

The laser-ablation matrix-isolation method for investigating transient reaction products has been described previously.[17] Early actinide metal atoms are reacted with H_2S to form actinide-bearing species in solid noble gas matrixes, which are identified and characterized from matrix-infrared spectra using $H_2{}^{34}S$ and $H_2{}^{32}S$, HDS, and D_2S mixtures. A

Received: March 5, 2013
Published: September 5, 2013

Table 1. Observed and Calculated Frequencies (cm^{-1}) for H_2ThS ($^1A'$) in C_s Symmetry[a]

experiment(Ar/Ne), B3LYP, PW91, CCSD(T)[b]				
H_2ThS	D_2ThS	$H_2Th^{34}S$	HDThS	mode assignment
1468.6/1488,[c] 1515.7 (367), 1504.0 (310), 1521.3	**1047.9**, 1074.5, 1066.2	**1468.6**, 1515.7, 1504.0	**1451.8**, 1494.2, 1485.5	Th−H str, a′
1435.3/1452,[c] 1471.3 (556), 1466.0 (475), 1480.9	**1025.2**, 1043.7, 1039.8	**1435.3**, 1471.3, 1466.0	**1036.7**, 1058.4, 1052.6	Th−H str. a″
464.8, 492.4 (191), 479.7 (166), 491.1	**454.3**, 462.6, 461.9	**453.4**, 489.5, 474.5	**457.6**, 471.0, 467.7	Th−S str, ThH_2 bend, a′
454.5 (59), 450.2 (42), 451.4	338.8, 327.1	446.6, 444.5	419.5, 404.2	ThH_2 bend, Th−S str, a′
386.5 (7), 365.6 (8), 388.1	278.0, 262.8	386.3, 365.3	358.0, 345.8	H−Th−S bend, a″
359.5(70), 345.5 (57), 359.6	261.3, 251.5	358.2, 344.3	273.6, 259.8	H−Th−S bend, a′

[a] Frequencies calculated in the harmonic approximation using the aug-TD basis set. [b] The order is argon matrix experimental values in bold followed by the calculated frequencies, (calculated intensities, km/mol) in the order **Experiment**, B3LYP, PW91, CCSD(T). Calculated intensities in km/mol given in parentheses. [c] Neon matrix frequencies are given after the slash.

Table 2. Observed and Calculated Frequencies for H_2US ($^3A''$) in C_s Symmetry[a]

experiment(Ar/Ne), B3LYP, PW91, CCSD(T)[b]				
H_2US	D_2US	$H_2U^{34}S$	HDUS	vib mode
1488.9/1511,[c] 1525.1 (402), 1498.4 (348), 1527.6	**1063.2**, 1081.1, 1062.2	**1488.9**, 1525.1, 1498.4	**1474.5**, 1527.8, 1483.5	U−H sym str, a′
1462.4/1482,[c] 1488.0 (556), 1468.2 (480), 1482.8	**1045.6**, 1055.5, 1041.2	**1462.4**, 1488.0, 1468.2	**1053.9**, 1082.6, 1051.5	U−H asym str., a″
476.9, 482.4 (159), 469.1 (137), 480.2	**468.4**, 468.9, 461.0	**466.2**, 476.0, 459.4	489.3, 463.9	U−S str, UH_2 bend, a′
459.3 (67), 437.0 (47), 452.5 (41)	330.1, 311.7	454.4, 435.3	402.9, 380.5	UH_2 bend, U−S str, a′
319.8 (3), 218.6 (98), 299.3	229.7, 158.6	319.5, 219.1	223.9, 188.9	H−U−S bend, a″
313.8 (92), 146.2*i*, 222.4	228.6, 104.0*i*	312.8, 146.2*i*	227.7, 121.8*i*	H−U−S bend, a′

[a] Frequencies calculated in the harmonic approximation using the aug-TD basis set. [b] The order is argon matrix experimental values in bold followed by the calculated frequencies, (calculated intensities, km/mol) in the order **Experiment**, B3LYP, PW91, CCSD(T). Calculated intensities in km/mol given in parentheses. [c] Neon matrix frequencies are given after the slash.

Continuum Minilite II Nd:YAG laser fundamental output (1064 nm, 15 Hz repetition rate with 5 ns pulse width) at 70% of maximum energy (56 mJ/pulse) was focused delivering about 10 mJ/pulse onto rotating thorium and uranium (Oak Ridge National Laboratory, high purity) targets, which produced bright emission plumes from the target surfaces that spread uniformly to the 4K CsI window. The H_2S sample (Matheson) was condensed and degassed, and deuterium enriched hydrogen sulfide was prepared by reacting FeS with H_2SO_4 diluted in D_2O. The sample of $H_2{}^{34}S$ was synthesized from sulfur-34 (98.8% ^{34}S, Cambridge Isotope Laboratories) reacting with pure iron powder forming $Fe^{34}S$ and then reacting with H_2SO_4 (4M). All prepared hydrogen sulfide gas samples were dried over fresh P_2O_5 powder.[18] FTIR spectra were recorded at 0.5 cm^{-1} resolution on a Nicolet 750 with 0.1 cm^{-1} accuracy using an MCTB detector. Matrix samples were annealed at different temperatures, and selected samples were subjected to photolysis by a medium pressure mercury arc lamp (Philips, 175W) with the outer globe removed.

The DFT calculations were done with the B3LYP[19,20] and PW91[21] functionals with the Gaussian 09 program system.[22] The basis set includes the aug-cc-pVTZ basis set on H and O,[23] the aug-cc-pV(T+d)Z basis set on S,[24] and a small core ECP (60 electrons in the core) with a (14s,13p,10d,8f,6g)/[10s,9p,5d,4f,3g] basis set on Th and U. Good general agreement has been found for frequencies calculated at the DFT level for open shell uranium bearing species such as triplet H_2UO, $CH_2{=}UH_2$ and $NH{=}UH_2$, and quintet UH_2 and HUF.[4,25−27] In the spin unrestricted calculations for triplet spin states of H_2UX, X = O, S, where the unpaired electrons reside in orbitals with 5f character, three unique low energy configurations with a specific set of orbital occupancies and spin and spatial symmetry (a′ × a′ = $^3A'$, a″ × a″ = $^3A'$, and a′ × a″ = $^3A''$) are possible, and it can be difficult to converge the wave function. Ultrafine grids were used in the DFT calculations as the use of the standard grids can change the M-H stretches by up to 40 cm^{-1}, even though the total energies do not change. The DFT frequencies for H_2ThS increased and those for H_2US decreased.

Subsequent calculations were done at the CCSD(T) level[28] with the same basis set with the open shell calculations done at the R/UCCSD(T) level.[29] This basis set at the CCSD(T) level has provided good vibrational frequencies for UO_2^{2+} and ThO_2.[30] Twelve electrons on the Th ($6s^2$, $6p^6$, $7s^2$, $6d^2$), 14 electrons on the U ($6s^2$, $6p^6$, $7s^2$, $6d^1$, $5f^3$), 1 electron on the H, and 6 electrons on the O or S were correlated. The CCSD(T) calculations were performed with the MOLPRO suite.[31]

■ RESULTS

Experimental results will be given first for thorium and then for uranium with the data summarized in Tables 1 and 2 respectively. The assignments to major product species are supported by the electronic structure calculations at the DFT level with the B3LYP and PW91 exchange-correlation functionals and at the correlated molecular orbital theory CCSD(T) level.

Thorium Spectra. Figure 1 illustrates infrared spectra for hydrogen sulfide reactions with laser ablated thorium atoms in excess argon. First, notice the sharp ThS absorption at 474.7 cm^{-1}, which is in agreement with its first observation from the thorium reaction with discharged elemental sulfur.[9] As shown in Figure 1a, broad new bands at 1468.6 cm^{-1} and at 1435.3 cm^{-1} appeared on deposition in the argon matrix. These bands were not affected by annealing to 20 K nor by >220 nm irradiation, Figure 1b,c. However, annealing to 30 and 35 K increased and sharpened both bands and produced other weaker features at 1459, 1456 cm^{-1} and at 1447 and 1420 cm^{-1} in the Th−H stretching region, and increased the ThS band and a much weaker band at 464.3 cm^{-1}, Figure 1d,e. The frequencies were not shifted in the Th−H stretching region for the $H_2{}^{34}S$ reaction, Figure 1f−j, but $Th^{34}S$ shifted to 462.3 cm^{-1} and the new band to 453.4 cm^{-1} in the Th−S stretching region. However, notice that annealing to 30 K straightaway after deposition increased and sharpened the product bands, Figure 1g, and produced the other features in the higher frequency region. Annealing to 35 K increased the product bands slightly, and further increase in the annealing temperature to 40 K had little effect, Figure 1i,j.

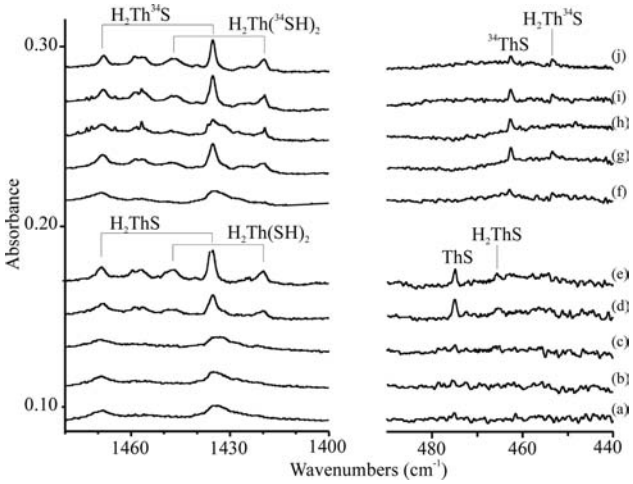

Figure 1. Infrared spectra from sample formed by co-deposition of laser ablated Th with 0.6% H_2S in argon: (a) 1 h sample deposition at 4 K, (b) after annealing to 20 K, (c) after 15 min >220 nm broad-band photolysis, (d) after annealing to 30 K, and (e) after annealing to 35 K and with 1.0% $H_2{}^{34}S$ in argon: (f) 1 h sample deposition at 4 K, (g) after annealing to 30 K, (h) 15 min >220 nm broad-band photolysis, (i) after annealing to 35 K, and (j) after annealing to 40 K. The absorbance scale is relative for each group of scans from different spectral regions.

Spectra from an approximately 50% deuterium enriched sample at a higher 1% concentration are illustrated in Figure 2; this sample, of course, contains more HDS than H_2S or D_2S. The deuterium enrichment was estimated from the H_2S and D_2S precursor infrared band intensities, normalized by calculated infrared intensities for these modes. The upper region contained the same 1468.6 and 1435.3 cm^{-1} bands plus a new intermediate band at 1451.8 cm^{-1} and new deuterium counterpart bands at 1047.9, 1036.6, and 1025.2 cm^{-1}. The lower region revealed a stronger ThS absorption, and both ThS_2 fundamentals[9] at 451.3 and 431.5 cm^{-1} plus an important new triplet absorption at 464.3, 457.6, 454.3 cm^{-1}. These bands increased on annealing to 30 and 35 K as before.

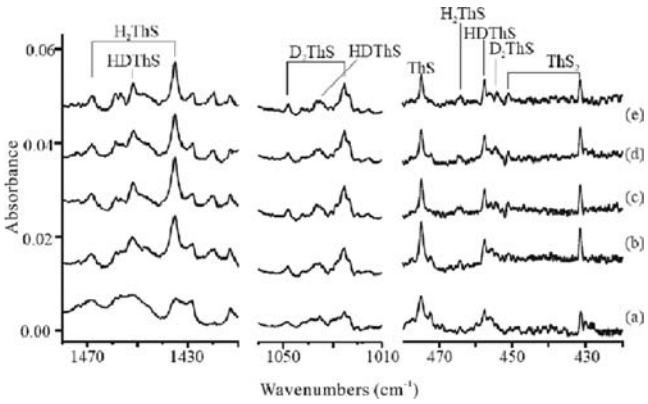

Figure 2. Infrared spectra from sample formed by co-deposition of laser ablated Th with 1.0% H_2S/HDS/D_2S with approximately 50/50 H/D in argon: (a) 1 h sample deposition at 4 K, (b) after annealing to 30 K, (c) after 15 min >220 nm broad-band photolysis, (d) after annealing to 35 K, and (e) after annealing to 40 K.

Experiments using 1% H_2S in excess neon and less laser energy gave weaker product bands at 1488 and 1452 cm^{-1}. These bands sharpened on annealing to 8 K, decreased on photolysis, and increased further on annealing to 10 K. Unfortunately, no new bands were detected in the lower region.

Uranium Spectra. The analogous reaction with uranium produced new broad features at 1488.9 and 1462.4 cm^{-1} and at 476.9 cm^{-1}, which sharpened and increased on annealing to 30 and 35 K, Figure 3(d,e). Other broader bands favored at higher annealing temperatures were observed at 1478 and 1447 cm^{-1}. Using isotopically labeled $H_2{}^{34}S$ as the reagent, Figure 3(f−j), again gave unshifted bands in the higher frequency region, but shifted in the lower frequency region, to 466.2 cm^{-1}. The bands increased on annealing to 30 K, and better focus of the >220 nm irradiation, Figure 3h, virtually destroyed these absorptions, which were restored on subsequent 35 K annealing.

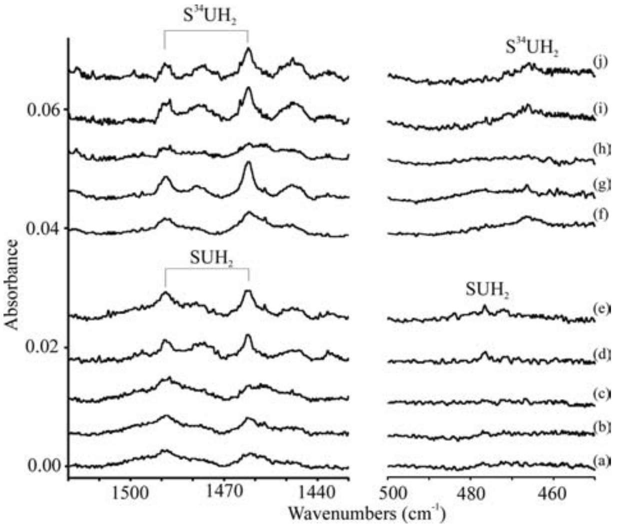

Figure 3. Infrared spectra from sample formed by co-deposition of laser ablated U with 0.8% H_2S in argon: (a) 1 h sample deposition at 4 K, (b) after annealing to 20 K, (c) after 15 min >220 nm broad-band photolysis, (d) after annealing to 30 K, and (e) after annealing to 40 K and with 0.6% $H_2{}^{34}S$ in argon: (f) 1 h sample deposition at 4 K, (g) after annealing to 30 K, (h) 15 min >220 nm broad-band photolysis, (i) after annealing to 35 K, and (j) after annealing to 40 K.

Spectra from a uranium experiment with a similar 1% mixture of H_2S, HDS, and D_2S in argon are illustrated in Figure 4. Triplet spectral features are observed in each region, at 1488.9,

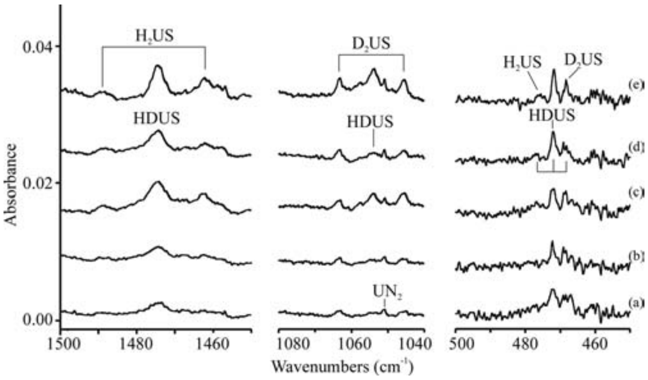

Figure 4. Infrared spectra from sample formed by co-deposition of laser ablated U with 1.0% H_2S/HDS/D_2S with approximately 50/50 H/D in argon: (a) 1 h sample deposition at 4 K, (b) after annealing to 20 K, (c) after annealing to 30 K, (d) after 15 min >290 nm broad-band photolysis, (e) after annealing to 35 K.

1474.5, 1462.4 cm^{-1}, at 1063.2, 1053.9, 1045.6 cm^{-1}, and at 476.9, 471.8, 468.4 cm^{-1}. The strongest US_2 band was observed at 438.7 cm^{-1} (not shown).[8]

Traces of UN_2 (1051 cm^{-1}), UO and UO_2 (820 and 776 cm^{-1})[32] were observed in these experiments, and the presence of these bands insures that the U ablation is working effectively. An experiment in excess neon produced new bands at 1511 and 1482 cm^{-1}, which sharpened on annealing to 10 K. The lower frequency region gave no new bands. No isotopic precursor reactions were investigated in neon.

Identification and Assignments for H_2ThS. The 1468.6 and 1435.3 cm^{-1} bands in solid argon track together on annealing and photolysis so they most likely belong to the same new molecule. Furthermore, they exhibit no S-34 shifts and large deuterium shifts to 1047.9 and 1025.2 cm^{-1} for bands that show similar annealing and photolysis behavior as the former two bands. Their frequency ratios of 1.401 and 1.400 are appropriate for heavy metal hydride stretching modes as ThH_2 itself has the 1455.6/1040.3 = 1.399 H/D ratio for the antisymmetric stretching mode.[33] The mixed H/D isotopic precursor reaction indicates that the 1468.6 and 1435.3 cm^{-1} bands are due to the two stretching modes of a ThH_2 subunit owing to the appearance of a single new intermediate band at 1451.8 cm^{-1} for a Th−H stretch and a similar band at 1036.6 cm^{-1} for a Th−D stretch between the ThD_2 subunit counterpart modes at 1047.9 and 1025.2 cm^{-1}. These intermediate bands, which track on annealing, are then the Th−H and Th−D stretching modes of the ThHD subunit of a new molecule. Their H/D ratio, 1.401, and their position within 0.1 cm^{-1} of the average of the above two stretching modes for ThH_2 and ThD_2 subunits support this assignment.

The weak 464.3 cm^{-1} band tracks with the 1468.6 and 1435.3 cm^{-1} bands on annealing and shifts to 453.4 cm^{-1} in the $H_2{}^{34}S$ reaction (Figure 1). This S-34 shift, 10.9 cm^{-1}, is slightly less than the 12.4 cm^{-1} shift for ThS itself,[9] which shows that this Th−S stretching mode is slightly mixed with other atoms in the molecule. The appearance of an almost 1/2/1 relative intensity triplet at (468.3, 457.6, 454.3) cm^{-1} in the mixed isotopic experiment with H_2S, HDS, D_2S precursor (Figure 2) demonstrates that two equivalent H atoms are bonded to the Th center and participate ever so slightly in the Th−S stretching mode, which, in fact, exhibits a 10.0 cm^{-1} deuterium shift. Thus, we have identified H_2ThS from the matrix infrared spectrum.

These assignments are confirmed by the electronic structure vibrational frequency calculations at the DFT level with the B3LYP and PW91 functionals and at the correlated CCSD(T) molecular orbital theory level. The predicted frequency results are compared to experiment in Table 1 for the ground $^1A'$ state of H_2ThS. (The DFT calculations with both functionals predict the lowest energy triplet state to be over 40 kcal/mol higher in energy than the singlet state). The optimized geometry parameters are shown in Table 3. First, the calculations show that the higher, weaker band is the symmetric ThH_2 stretching mode and the lower, stronger band is the antisymmetric counterpart. The CCSD(T) calculations predict the two modes to be 53 cm^{-1} and 46 cm^{-1} too high for the Ar spectra. Comparison of the CCSD(T) results with the Th−H stretches in Ne reduces the error in the symmetric stretch to 33 cm^{-1} and the error for the antisymmetric stretch to 29 cm^{-1}. The B3LYP functional predicts the symmetric stretch to be 47 cm^{-1} too high and the antisymmetric stretch 36 cm^{-1} too high for the Ar matrix spectra. The PW91 functional predicts the symmetric and antisymmetric stretches to be 35 cm^{-1} and 31 cm^{-1} too high, respectively, as compared to the Ar spectra. The differences between the DFT frequencies and experiment decrease as well in comparison to the Ne matrix results. The computational results which are harmonic frequencies are in very good agreement with experiment for the Th−H stretching modes of H_2ThS, considering the neglect of anharmonicity in the calculations. As a benchmark, our CCSD(T) calculation for the ground $^1A_1$ state of ThH_2 (Table 4) predicts the stretching modes to be 56 cm^{-1} and 51 cm^{-1} too high as compared to experiment for the Ar matrix and by 31 cm^{-1} for the antisymmetric stretch in the Ne matrix, essentially the same differences as found for H_2ThS. The results clearly show that the ground state for H_2Th is the singlet, which the PW91 functional incorrectly finds as the triplet. Both DFT functionals predict the Th−H and Th−D stretching modes for HDThS to be within 1 cm^{-1} of the average of the symmetric and antisymmetric values for the pure isotopic species H_2ThS and D_2ThS as found from experiment.

Table 3. Optimized Geometry Parameters for the H_2MS (M = Th, U) Molecular Ground States

property	PW91	B3LYP	CCSD(T)
	H_2ThS (C_s − $^1A'$)		
r(Th−S) Å	2.378	2.389	2.396
r(Th−H) Å	2.059	2.067	2.070
∠S−Th−H °	99.9	101.7	101.0
∠H−Th−H °	100.2	101.0	102.7
	H_2US (C_s − $^3A''$)		
r(U−S) Å	2.326	2.336	2.334
r(U−H) Å	1.997	2.004	2.010
∠S−U−H °	98.6	101.6	104.7
∠H−U−H °	97.4	98.7	102.4

The mode at 464.3 cm^{-1} is an out-of-phase coupling of symmetric Th−S stretching and ThH_2 bending modes, and it is predicted to be ∼40 cm^{-1} higher than the weaker in-phase counterpart, which we cannot observe in our experiment because of the lower frequency and weak intensity. The CCSD(T) value for this mode is 30 cm^{-1} larger than experiment. The B3LYP and PW91 functionals predict values that are 28 cm^{-1} and 15 cm^{-1} too high, respectively, as compared to experiment in the Ar matrix. As a benchmark, our CCSD(T) calculation predicts (Table 5) the stretch in diatomic ThS to be 4 cm^{-1} above the 474.7 cm^{-1} argon matrix value, with B3LYP predicting values a few cm^{-1} higher so the Th−S stretch is being determined correctly. The B3LYP functional overestimates the H motion based on the D isotopic shift and underestimates the S motion based on the S-34 shift, but it correctly predicts the HDThS subgroup mode position in the lower band (the HDThS band is 6.2 cm^{-1} below the H_2ThS, D_2ThS isotopic average). The PW91 functional finds this coupled mode to be lower than the B3LYP value (a characteristic of PW91) and thus closer to the observed value, and predicts a smaller D isotopic shift and a larger S-34 shift, which are closer to the observed values. The HDThS counterpart is calculated 3.1 cm^{-1} below the pure isotopic species average, and it is observed 1.7 cm^{-1} lower.

The broad bands at 1447 and 1420 cm^{-1} favored on higher annealing cycles appear in the Th−H stretching region and exhibit no S-34 shifts, but clear deuterium counterparts are not observed in the mixed H/D isotopic spectra. These bands are most likely due to secondary reaction products involving a

Table 4. Calculated Values for the MH_2 Molecular Ground States[a]

property	PW91	B3LYP	CCSD(T)	Expt(Ar/Ne)
		ThH_2 ($^1A_1$)		
r(Th–H) Å	2.007	2.016	2.031	
∠H–Th–H °	123.8	125.2	125.0	
Th–H sym. str. (a_1)	1542.2 (71)	1550.5 (87)	1536.5	1480
Th–H asym. str. (b_2)	1498.9 (416)	1500.5 (513)	1506.7	1455.6/1476.0
H–Th–H bend (a_1)	523.8 (5)	552.8 (5)	606.5	
		ThH_2 ($^3B_1$)		
ΔE($^1A_1$-$^3B_1$) (kcal/mol)[b]	−0.6	2.9	7.1	
r(Th–H) Å	2.051	2.056	2.062	
∠H–Th–H °	112.3	114.7	116.9	
Th–H sym. str. (a_1)	1485.3 (161)	1469.6 (188)	1508.6	
Th–H asym. str. (b_2)	1462.1 (518)	1430.9 (653)	1461.5	
H–Th–H bend (a_1)	489.4 (44)	495.1 (41)	513.5	
		UH_2 ($^5B_2$)		
r(U–H) Å	2.042	2.057	2.054	
∠H–U–H °	105.7	108.4	108.2	
U–H sym. str. (a_1)	1437.0 (287)	1452.4 (291)	1459.3	1406
U–H asym. str. (b_2)	1391.7 (474)	1395.7 (606)	1399.7	1370.7/1403.5
H–U–H bend (a_1)	396.1 (103)	388.7 (116)	418.8	

[a] aug-TD basis set. [b] The $^3B_1$ state is 7.1 kcal/mol above the ground $^1A_1$ state at the CCSD(T) level and 2.3 kcal/mol higher at the B3LYP level. At the PW91 level, the $^3B_1$ state is the ground state with the $^1A_1$ state 1.3 kcal/mol higher in energy.

Table 5. CCSD(T)/aug-TD Values for the MX (M = Th, U; X = O, S) Diatomic Molecular Ground States[a]

property	^{1}ThO	^{5}UO[b]	^{1}ThS	^{5}US[b]
r(Th–X) Å	1.8453	1.8452	2.3556	2.3794
Th–X str. (σ) cm^{-1}	888.8	834.5	478.7	446.7
anharmonicity cm^{-1}	2.28	0.70	0.90	1.01
ΔE (kcal/mol)	19.2	4.0	14.1	6.3

[a] Data obtained from a 5-point fit. [b] The ground states of UO and US are quintet states. The spatial state description is more difficult to assign because of the use of only C_{2v} symmetry and the lack of spin orbit corrections. Our initial assignment for UO is a Δ state.

second H_2S molecule. B3LYP and PW91 calculations for the singlet ground state state $H_2Th(SH)_2$ molecule given in Supporting Information, Table S1 predict Th–H stretching modes near those for H_2ThS, as expected, and these weaker bands are tentatively assigned to this secondary reaction product.

Identification and Assignments for H_2US. The stronger 1488.9, 1462.4, and weaker 476.9 cm^{-1} bands show similar intensity changes on annealing and photolysis so they likely belong to the same new molecule. These bands increase on annealing to 30 K and decrease on >220 nm irradiation, best shown at the top of Figure 3, and they are more photosensitive than the Th species. These bands exhibit well-defined deuterium counterparts at 1063.2 and 1045.6 cm^{-1} as shown in Figure 4, which give 1.400 and 1.399 H/D frequency ratios, again appropriate for a heavy metal hydride vibration. The UH_2 molecule antisymmetric stretching mode isotopic frequency ratio 1370.7/978.7 = 1.401 is almost the same.[34,35] The mixed H/D precursor reaction also reveals stronger intermediate bands for the mixed isotopic product with an HUD subunit. Notice that the 1474.5 cm^{-1} intermediate band is twice as intense as the 1053.9 cm^{-1} deuterium counterpart, as are the computed isotopic intensity ratios (Table 2), and the frequency ratio is 1.399 as expected for U–H and U–D stretching modes even in the same HUD subunit. Again, calculations show that the upper band is the symmetric and the lower band is the antisymmetric U–H stretching mode in a UH_2 subunit, and their relative intensities are in qualitative agreement with experiment.

The weaker 476.9 cm^{-1} band shifts to 466.2 cm^{-1} with S-34, and this 10.7 cm^{-1} shift is just less than the 11.9 cm^{-1} shift for US itself.[8] Again a clear mixed H/D isotopic triplet is observed for the uranium product at 476.9, 471.8, 468.4 cm^{-1}, which verifies that two equivalent H atoms are involved in this mostly U–S stretching mode. Hence, the assignment of H_2US as the major uranium–hydrogen sulfide product is straightforward.

The lowest energy spin state for H_2US is derived from the f^2 occupancy, and, as discussed above, there are three triplet configurations possible that can be calculated with single configurations, $^3A'$, $^3A''$, and a second $^3A'$. At the DFT level with the B3LYP and PW91 functionals and at the CCSD(T) level, the $^3A''$ state is the ground state (geometry parameters in Table 3). We note that the ordering of the energies depends on the basis set and that calculations with smaller basis sets without g functions on the U gave $^3A'$ derived from a′ × a′ as the ground state. At the CCSD(T) level, the $^3A'$ (a′ × a′) state is 1.4 kcal/mol higher in energy and the other $^3A'$ (a″ × a″) state is 3.3 kcal/mol higher in energy. The corresponding energy differences at the B3LYP level are 0.5 and 3.3 kcal/mol and are 1.7 and 2.9 kcal/mol with the PW91 functional. The spin expectation values at the DFT levels are close to 2.0 (Supporting Information, Tables S3, S4), which shows that there is little spin contamination in these triplet states. H_2UO has the same ordering of electronic states with the $^3A''$ state as the ground state followed by the $^3A'$ (a′ × a′) state higher in energy by 1.5, 1.0, and 1.1 kcal/mol and with the $^3A'$ (a″ × a″) state higher in energy by 3.1, 3.5, and 3.7 kcal/mol at the CCSD(T), PW91, and, B3LYP levels, respectively.

Table 2 lists frequencies computed for the ground $^3A''$ state using CCSD(T) and both DFT functionals. The CCSD(T) calculations predict the symmetric U–H stretch to be 39 cm^{-1} too high and the antisymmetric U–H stretch to be 20 cm^{-1} too high for the ground $^3A''$ state as compared to the Ar matrix results. The differences between the CCSD(T) calculations and the Ne results decrease to 17 cm^{-1} and 1 cm^{-1} for the symmetric and antisymmetric U−H stretches. The B3LYP functional predicts the a′ U−H stretch to be 36 cm^{-1} too high and PW91 functional predicts it to be 10 cm^{-1} too high compared to the Ar matrix results. The a″ U−H stretch is predicted to be 26 cm^{-1} too high at the B3LYP level and 6 cm^{-1} high at the PW91 level relative to the Ar matrix results. The PW91 functional predicts U−H stretches that are too low as compared to the Ne matrix values. The differences from experiment for the CCSD(T) and B3LYP results are consistent with comparison of calculated harmonic values with anharmonic experimental values. The CCSD(T) calculations predict the coupled US stretch plus UH_2 bend to be 3 cm^{-1} too high, B3LYP gives a value 6 cm^{-1} too high, and PW91 predicts a value 8 cm^{-1} too low as compared to experiment. This mode is an out-of-phase coupling of symmetric U−S stretching and UH_2 bending modes. The predicted frequencies for the two $^3A'$ states are comparable to those for the $^3A''$ ground state in the observed region, consistent with the similar state energies.

There are a number of low-lying states for UH_2 as well. The ground state for UH_2 is the $^5B_2$ state derived from the ($a_1 \times a_1 \times a_1 \times b_2$) occupancy. The next nearest state is $^5A_2$ derived from the ($a_1 \times a_1 \times b_1 \times b_2$) occupancy, which is 2.1 kcal/mol higher in energy at the CCSD(T) level. The CCSD(T) values for the symmetric and antisymmetric stretches are 53 and 29 cm^{-1} too high, respectively, as compared to the Ar matrix values (Table 4) The differences from the Ar experimental values are comparable to those for H_2US further confirming the reliability of the CCSD(T) calculations. However, the CCSD(T) antisymmetric stretch is within 4 cm^{-1} of the Ne matrix value.[35]

The other broad bands at 1478 and 1447 cm^{-1} favored on higher annealing cycles appear in the U−H stretching region and exhibit no S-34 shifts, and clear deuterium counterparts are not observed in the mixed H/D isotopic spectra. The annealing behavior suggests that these bands are due to secondary reaction products involving a second H_2S molecule. Our DFT calculations for the higher order product $H_2U(SH)_2$ (Supporting Information, Table S2) predict strong bands in this region for U−H stretching modes of such an aggregate species. Even though we may not have located the lowest triplet spin state for this aggregate species, our calculations for H_2US show that there is little frequency variation among the lowest spin states, and the results in Supporting Information, Table S2 are adequate to support this tentative assignment.

Bonding Considerations. It is interesting to compare the stretching modes observed for the major H_2ThS and H_2US products in solid argon and neon. Typically the neon matrix host gives frequencies that are higher by a few cm^{-1}, but stronger matrix interactions will lead to larger matrix shifts.[36] An extreme case is CUO, where the two observed vibrational modes increase by 8.5% and 23% on the change of ground electronic states between solid argon and neon.[37,38] The two Th−H stretching modes of H_2ThS are 19 and 17 cm^{-1} higher in solid neon and the two U−H stretching modes of H_2US are 22 and 20 cm^{-1} higher in solid neon. These M-H stretches can be compared with the antisymmetric stretching mode of UH_2 in solid argon at 1370.7 cm^{-1}, which shifts to 1403.5 cm^{-1} in solid neon,[34,35] and the antisymmetric stretching mode of ThH_2 in solid argon at 1455.6 cm^{-1}, which shifts to 1476.0 cm^{-1} in solid neon (Table 4).[39] It appears that there is a sizable matrix interaction with actinide species, which is responsible for the 17−22 cm^{-1} argon−neon matrix shifts (1−2%), but these shifts are modest, and it is unlikely that there is a change in electronic states from argon to neon matrix hosts for these species. This surely applies to the lowest spatial/spin states for the uranium species as well, which are spread over a 3 kcal/mol range.

It is important to compare the actinide-hydrogen stretching modes for the dihydride sulfides with the corresponding isostructural dihydride oxides observed previously,[3,4] and to seek an explanation for the 71−85 cm^{-1} *higher* hydrogen-actinide stretching frequencies observed here for the sulfides over the oxides. Here the An-H stretching frequencies provide reliable insight for these species as they are much higher than other frequencies and therefore not mixed with other modes. The U−H stretching modes in H_2UO and H_2US are *higher* than the 1406.1 and 1370.7 cm^{-1} values for the two U−H stretching modes observed for UH_2 itself in solid argon. In contrast, the Th−H stretching counterparts in H_2ThS are *lower* than the 1480.1 and 1455.6 cm^{-1} values found for ThH_2 isolated in solid argon.[34,35] Table 6 presents relevant observed An-H stretching frequency data to facilitate these comparisons.[26,27,40] Thus, the sulfide and oxide substituents affect UH_2 and ThH_2 differently.

Table 6. AnH_2 Stretching Frequencies Observed in Solid Argon for the ThH_2 and UH_2 Molecules and Subgroups in Other Small Molecules and AnH and AnH_4 for Comparison

molecule	frequencies[a]	molecule	frequencies[a]	references
ThH_2 ($^1A_1$)	1480, 1456			33, 39
H_2ThS ($^1A'$)	1469, 1435	H_2US ($^3A''$)	1489, 1462	this work
$^1CH_2ThH_2$	1436, 1397	$^3CH_2UH_2$	1461, 1426	26, 43
$^1HNThH_2$	1399, 1357	$^3HNUH_2$	1436, 1403	27, 40
H_2ThO ($^1A'$)	1397, 1352	H_2UO ($^3A''$)	1416, 1377	3, 4
		UH_2 ($^5A_2$)	1406, 1371	25, 34
^2ThH	1485	^4UH	1424	33, 34
ThH_4 ($^1A_1$)	1445 (antisym)	$^3UH_4$	1484 (antisym)	33, 34

[a] Frequencies rounded to nearest cm^{-1} and listed in symmetric, antisymmetric order.

First, the dihydride oxides were recalculated with the same methods as used for the sulfides (Table 7). The ground state of H_2UO is the $^3A''$ state just as found for the sulfide. The $^3A'$ ($a' \times a'$) state is 1.5 kcal/mol higher in energy at the CCSD(T) level with the $^3A'$ ($a'' \times a''$) state 3.1 kcal/mol above the $^3A''$ state. The same states and comparable structures were obtained using ADF 2.3 calculations.[3,4] The U−H bonds are calculated to be 0.04 Å longer in the oxide than in the sulfide. The same lengthening of 0.04 Å is predicted for the Th−H bonds from the sulfide to the oxide. The symmetric stretching frequency is 60 cm^{-1} *higher* for the $^1A'$ sulfide than for the oxide for the thorium compounds at the CCSD(T) level and the antisymmetric Th−H stretch is a comparable 66 cm^{-1} higher in the sulfide. Second, in the H_2US case the mixed U−S stretching mode is 26 cm^{-1} *higher* than the value for US diatomic observed previously,[8] and the U−H stretching modes are 83 and 91 cm^{-1} *higher* than the values observed for UH_2.[34,35] For H_2ThS, the mixed Th−S stretching mode is 10 cm^{-1} *lower* than the value for ThS and the Th−H stretching modes are 11 and 21 cm^{-1} lower than observed for ThH_2.[9,33] The present and earlier calculated bond lengths[8,9] are

Table 7. CCSD(T)/aug-TD Values for the H_2MO (M = Th, U) Molecular Ground States

Property	PW91	B3LYP	CCSD(T)
H_2ThO (C_s − $^1A'$)			
r(Th−O) Å	1.862	1.861	1.870
r(Th−H) Å	2.096	2.107	2.112
∠O−Th−H °	103.7	105.2	105.4
∠H−Th−H °	99.2	100.4	102.7
Th−H sym. str. (a′)	1451.9 (299)	1456.4 (338)	1461.4
Th−H asym. str. (a″)	1406.3 (572)	1404.7 (673)	1415.2
Th−O str. (a′)	848.3 (230)	856.8 (274)	841.6
H−Th−H bend (a′)	461.9 (77)	475.3 (97)	470.5
H−Th−O asym. bend (a″)	373.4 (1)	385.9 (2)	396.3
H−Th−O sym. bend (a′)	332.5 (161)	337.3 (204)	345.8
H_2UO (C_s − $^3A''$)			
r(U−O) Å	1.819	1.814	1.814
r(U−H) Å	2.050	2.056	2.051
∠O−U−H °	113.3	110.1	106.9
∠H−U−H °	99.0	100.8	102.6
U−H sym. str. (a′)	1438.7 (308)	1466.0 (349)	1473.8
U−H asym. str. (a″)	1392.2 (559)	1404.9 (658)	1409.7
U−O str. (a′)	857.1 (228)	878.7 (277)	875.6
H−U−H bend (a′)	475.5 (70)	478.7 (81)	479.3
H−U−S asym. bend (a″)	194.5 (33)	257.2 (21)	289.0
H−U−O sym. bend (a′)	191.9 (255)	251.1 (267)	225.5

consistent with this U−S and Th−S stretching frequency relationship.

The relevant molecular orbitals for the H_2US and H_2ThS products are compared with their oxide relatives in Figures 5 and 6, respectively. Alpha spin orbitals are plotted for the $^3A''$ H_2US and H_2UO species and electron pair orbitals for $^1A'$ H_2ThS and H_2ThO. The alpha and beta spin orbitals are similar showing that there is not a large spin polarization effect. An electron density of 0.04 e/au^3 was chosen to show the differences between the softer sulfide and harder oxide substituents. Owing to the higher electronegativity of O, the $2p^2$ lone pair electrons are localized on the O center, but in contrast the S 3p electrons in the π system are more delocalized back-bonding through an empty U 6d orbital on the metal center and to reach the H centers, and *thus contribute to shortening the U−H bonds and increasing the U−H stretching frequencies.* In the sulfides this additional bonding arises from the highest energy doubly occupied π molecular orbital shown in Figure 5. In addition, the sulfur 3p orbitals are also mixed with the two singly occupied f orbitals showing a role for the f orbitals in the bonding.

We performed a natural bond orbital (NBO) analysis[41] at the B3LYP level of theory for the $^3A''$ ground state H_2US, and the condensed NBO populations are given in Table 8. UO and US are U(II) formally with a d^1f^3 configuration. In actuality, the electron configuration is $s^{0.9}d^{0.9}f^{3.1}$ for UO and $s^{1.0}d^{1.0}f^{3.1}$ for US. This shows that there is slightly more back-donation from the S than from the O to the U. It also shows that there is a minor role for the 5f orbitals in the bonding to the O or S as there is slightly more 5f character than expected from the d^1f^3 configuration. In contrast, the U in H_2UO and H_2US is formally U(IV) with an f^2 configuration. The electron configuration on U is $s^{0.4}d^{1.2}f^{2.6}$ for H_2UO and $s^{0.4}d^{1.7}f^{2.5}$ in H_2US. In both cases, the 5f population is more than expected from the configuration so there is a clear role for the 5f orbitals in binding to the H and O or S. This is clearly seen in the MO diagrams of the two singly occupied molecular orbitals (SOMOs). Again, there is more back-bonding from the S than there is from the O. Qualitatively we have the same B3LYP results for US as reported in a recent work.[14] The U−H bonds in H_2US are more covalent than in H_2U on the basis of the NBO population analysis. There is also more f character in the U−H bonds in H_2US. The unpaired electrons in H_2US are essentially pure 5f orbitals with a small amount of 6d character (<3%). Here, we agree with Marsden et al.[14] that 5f orbitals make a contribution to the bonding in UO, which contains a polarized triple bond, and this contribution is significantly larger for H_2UO. The analogous mixed oxide, fluoride F_2UO was recently described in like manner to have a polarized triple bond using the CASPT2 method.[42]

The condensed NBO populations and bonding for H_2ThS and H_2ThO in Table 8 reveal further insights. The Th centers in ThO and ThS are formally Th(II) and there is actually a bit more 5f orbital participation in the backbonding on the Th than on the U for the diatomics. The 5f orbital participation for H_2ThX (X = O, S) increases by ~0.1 e from the diatomic. It appears that the more electronegative O withdraws more charge from Th thus contracting the 5f orbitals and making them more accessible for bonding.

It is not readily obvious why substitution at the metal increases the UH_2 stretching frequencies (decreases the bond lengths) and decreases the ThH_2 frequencies (increases the bond lengths) starting from the triatomic dihydride values, as shown in Tables 4 and 6.[43,44] ThH_2 and several observed substituted species derived from it are singlet states, whereas UH_2 is a quintet and all of the substituted species are triplet states. The lone pair for ThH_2 resides in a hybrid with 75% s and 24% d character. For UH_2, three of the unpaired electrons are in 5f orbitals (one of which has 5% s character) and the remaining electron is in a hybrid with 66% s, 25% d, and 5% f character. It appears that the repulsion between the nonbonded electrons and the U−H bond pairs should be decreased in the triplet state products allowing an increase in the triplet product UH_2 stretching frequencies. For ThH_2 the more electronegative

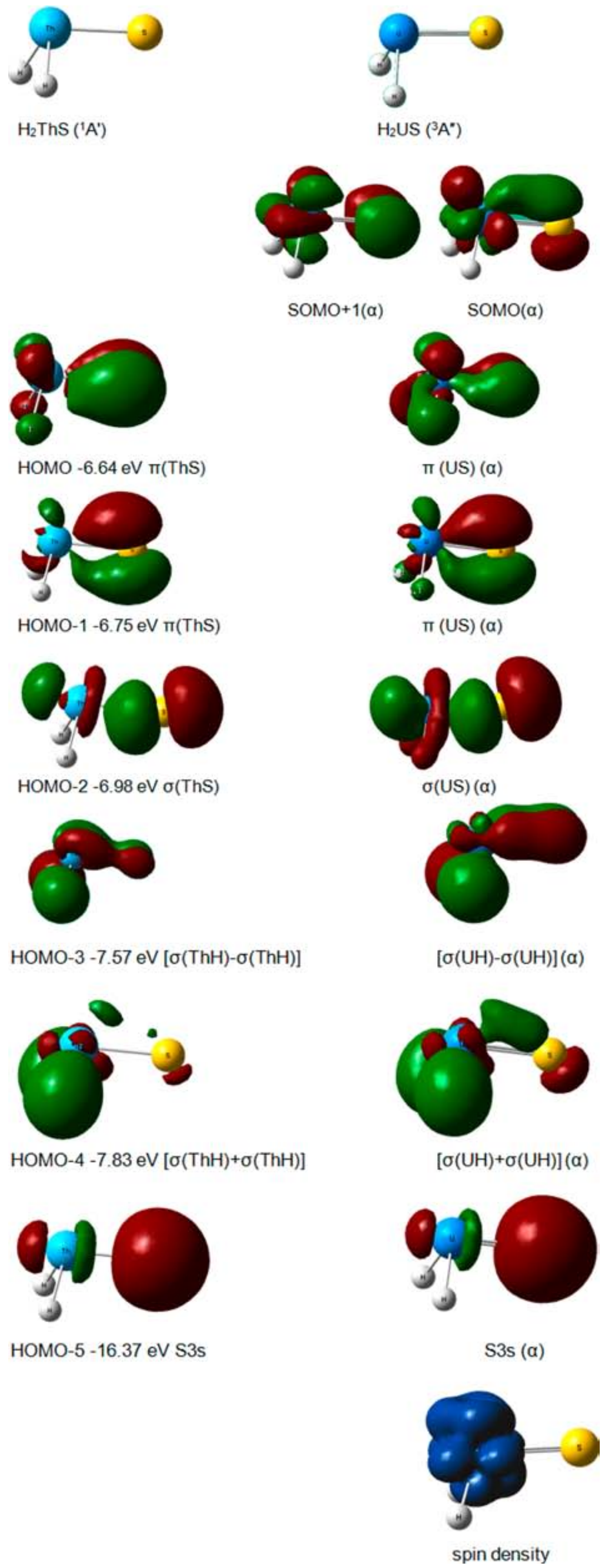

Figure 5. Comparison of *σ* and *π* molecular orbitals calculated for the H_2ThS and H_2US molecules using the B3LYP functional with an iso-electron density contour of 0.04 e/au^3. Alpha spin orbitals are plotted for the U $^3A''$ species and doubly occupied orbitals are plotted for the Th $^1A'$ species. The higher energy polarized *π* molecular orbitals for An-S are delocalized over the H centers, but the corresponding *π* molecular orbitals for An-O are not so delocalized, as shown in Figure 6.

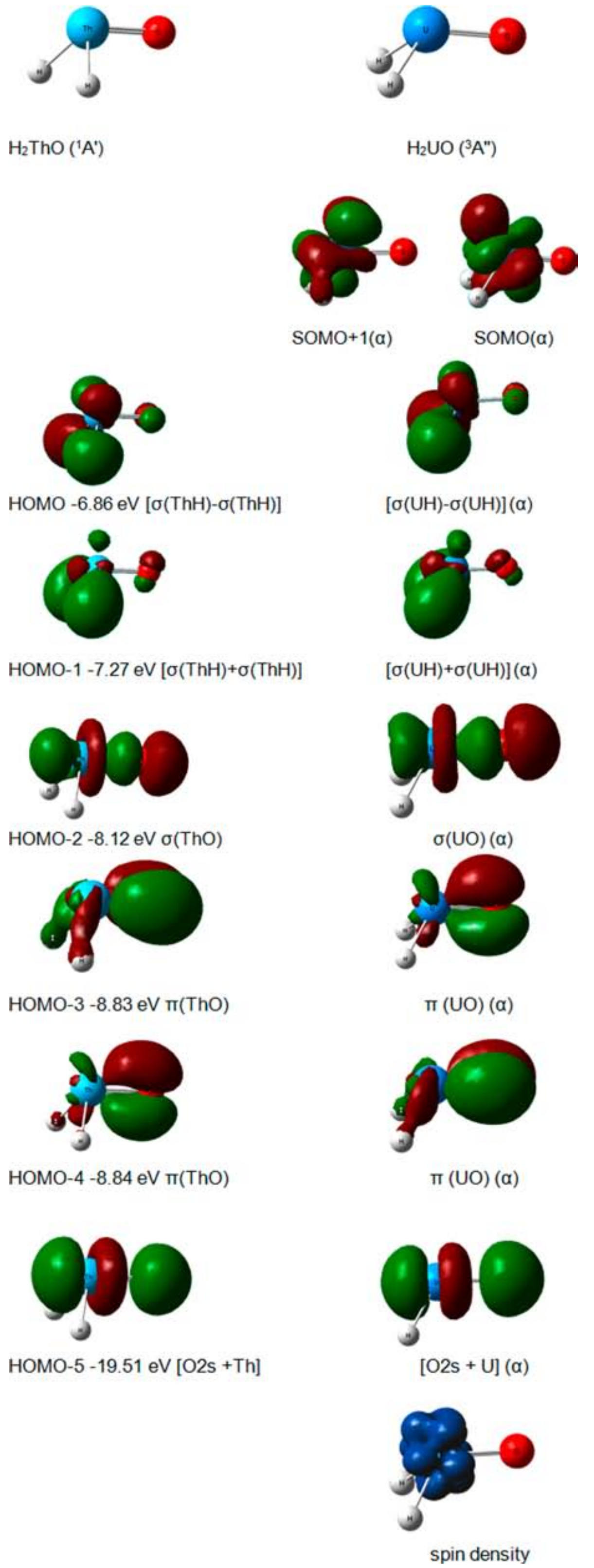

Figure 6. Comparison of *σ* and *π* molecular orbitals calculated for the for H_2ThO and H_2UO molecules using the B3LYP functional with an iso-electron density countour of 0.04 e/au^3. Alpha spin orbitals are plotted for the U $^3A''$ species and electron pair orbitals are plotted for the Th $^1A'$ species.

substituents may assist removal of electron density from the Th−H bonds thus allowing a decrease in the singlet product

Table 8. Natural Electron Configuration on Th and U Metals and Charges on all Elements Calculated at the B3LYP Level of Theory

molecule	M(7s)	M(7p)	M(6d)	M(5f)	q(M)	q(E)	q(H)
ThO	1.84	0.10	0.71	0.34	1.10	−1.10	
ThS	1.80	0.06	1.18	0.24	0.77	−0.77	
UO	0.93	0.07	0.88	3.10	1.07	−1.07	
US	0.95	0.06	1.03	3.10	0.88	−0.88	
H_2Th	1.62	0.04	1.21	0.17	0.99		−0.49
H_2U	0.97	0.05	0.85	3.06	1.09		−0.54
H_2ThO	0.36	0.10	1.28	0.39	1.99	−1.02	−0.48
H_2ThS	0.42	0.08	1.72	0.31	1.56	−0.69	−0.43
H_2UO	0.35	0.10	1.21	2.61	1.81	−0.86	−0.47
H_2US	0.43	0.10	1.66	2.54	1.32	−0.56	−0.38

ThH_2 stretching frequencies. ThS has been reported to have about a 20 kcal/mol higher bond dissociation energy than does US,[14] and thus the addition of S at the Th site in ThH_2 will have a larger impact than addition of S to the U in UH_2. We find only opposing trends in An-H bond polarity, metal character, metal s, or metal d contributions for the frequency increases with each metal.

The NBO analysis suggests a highly polarized triple bond character for both An-S bonds. The triple bonds have more metal character in the US bond than in the ThS bond with the difference showing up mostly in the π bonds. There is more f character in the US π bonds than in the ThS π bonds and conversely there is more d character in the ThS π bonds. The larger amount of f character in the US bonds and the larger amount of d character in the ThS bonds are consistent with the atomic configurations. The approximate bond orders of 3 for the ThS bond in H_2ThS and the US bond in H_2US are consistent with the polarized 2.89 oxo bond order found for F_2UO using a CASSCF approach.[42] A similar F substituent bonding effect is found for the terminal nitrides and phosphides $N{\equiv}UF_3$ and $P{\equiv}UF_3$ where the U−F bond lengths have been computed as 2.046 and 2.039 Å, respectively, at the CASSCF/CASPT2 level.[45]

What effect do the two H substituents on the U center have on the empty 5f orbitals that might make them more receptive to back-bonding from S 3p electrons? The natural charges calculated at the B3LYP level are given in Table 8. The values show that the full ionic model for the bonding is not exact for either H_2US or US. The addition of the two hydrogens to US increases the positive charge at the U center, and this will contract the U 6d orbitals and make them more receptive to back-bonding. If increased positive charge at the U center is important, then a comparison of US and US^+ might provide more useful information. Recent DFT calculations at the B3LYP level on US predicted a bond length of 2.374 Å and harmonic frequency of 450 cm^{-1} and corresponding values of 2.322 Å and 483 cm^{-1} for US^+.[14] These values are strikingly close to what we found for US (451 cm^{-1} observed in solid Ar)[8] and for H_2US here (476.9 cm^{-1} observed in solid Ar). We believe that these numbers and our higher calculated natural charge of 1.69 on U for quartet US^+ (Supporting Information, Table S6) show convincingly that the H substituents on the U center increase the positive charge at U, which should contract the 5f orbitals and increase their participation in bonding to S in H_2US. Clearly both US^+ and H_2US contain substantial polarized triple bond character. The polarized higher energy US and ThS π molecular orbitals in H_2MS, which are delocalized over the H centers (Figure 5), shorten the U−H and Th−H bonds and increase their vibrational frequencies.

For the thorium case, the Th−H bonds are computed to be about 0.04 Å shorter and the stretching frequencies 53−61 cm^{-1} *higher* for the sulfides than for the oxides, but the mixed terminal H_2Th−S stretching mode is 10 cm^{-1} *below* the value for diatomic ThS.[9] This is also the case for H_2ThO, where the Th−O mode is below the diatomic value (in this case by 54 cm^{-1}).[3] The π molecular orbitals again show delocalization of a S 3p nonbonding pair over the H centers, which is augmented by the pyramidal structure and strengthens the Th−H bond in the sulfide, Figure 5. Again, natural charges were calculated at the B3LYP level for both H_2ThS and ThS (Table 8). These values show that the addition of hydrogen does increase the positive charge at the Th center. A recent B3LYP calculation predicted ThS^+ to have a shorter bond, 2.311 Å and a higher harmonic frequency, 514 cm^{-1}, than ThS, 2.347 Å and 489 cm^{-1}.[14] A similar trend was found for ThO and ThO^+.[14,46] Clearly, the increase of positive charge at the Th center increases the Th−S stretching frequency in the simple diatomic molecule. In the case of H_2ThS, there is mixing of the Th−S stretch with the ThH_2 bend, more than found for the corresponding mixing in H_2US, which decreases the former normal-mode frequency and makes the Th−S frequency less descriptive of the bonding effects than its bond length. There is a smaller D shift for the predominantly actinide-sulfur stretching mode for H_2US (8.5 cm^{-1}) than for H_2ThS (10.0 cm^{-1}). Although the S 3p back-bonding does increase the Th−H stretching frequencies, this effect with Th is slightly less than we found with U. The back-bonding π molecular orbitals, shown in Figure 5, appear to be similar for Th as for U. In the analogous $N{\div}ThF_3$ and $P{\div}ThF_3$ species, we note that the Th−F bond is computed to be 0.006−0.009 Å shorter and the Th−F stretching frequencies observed to be 2−3 cm^{-1} higher in the phosphide species.[47]

How strong is this enhanced metal hydride bonding effect? The pyramidal structures of H_2ThS and H_2US clearly bring the H atoms closer to the delocalized dative π bond, which allows their overlap and sustains this enhanced metal hydride bonding effect. We recalculated the structures of H_2ThS and H_2US under imposed C_{2v} symmetry, which prevents this favorable metal hydride interaction with the dative π bond. It has been noted in the cases of H_2ThO and H_2UO that the pyramidal structures allow for the more effective use of both the U 5f and 6d orbitals in the bonding of the H and O atoms.[3,4] The planar C_{2v} structures for these actinide hydride oxides were predicted to be 6 and 5 kcal/mol higher in energy, respectively, with the PW91 functional and the basis sets and relativistic approaches implemented in the ADF code.[3,4,48] Here we further demonstrate that the oxides do not contain the delocalized dative bond exhibited by the sulfides, which is responsible for the enhanced bonding effect. Thus, the increased stability of H_2ThO and H_2UO in the pyramidal structures can be attributed mostly to increased localized bond strengths. The lowest planar H_2ThS ($^1A_1$), H_2ThO ($^1A_1$), H_2US ($^3A_2$), and H_2UO ($^3A_2$) structures are 8, 6, 16, and 11 kcal/mol higher in energy, respectively, at the B3LYP level than the pyramidal ground state conformers. There are, of course, other low lying spin states for planar H_2US and H_2UO as there are multiple low-lying states for the pyramidal structures, but these other spin states have no effect on the present discussion. We suggest that these energies contain a contribution from the delocalized π enhanced metal hydride bonding effect for the sulfides, but we cannot apportion changes for the localized bond energies with structure.

The structures and relevant molecular orbitals are illustrated in Supporting Information, Figure S1 for the planar subject molecules, and the frequencies and bond lengths are given in Supporting Information, Table S7. Note the imaginary frequencies for the out-of-plane bending modes of these transition state structures. The dative U−S π and U−H σ molecular orbitals do not overlap in the planar structure. As a result the U−H bond lengthens by 0.05 Å and the calculated U−H frequencies are 104 cm^{-1} and 92 cm^{-1} lower for the symmetric and antisymmetric stretches, respectively, in the planar structure. The corresponding changes for planar H_2ThS are an increase of 0.05 Å for r(Th−H) and corresponding decreases of 84 and 130 cm^{-1} for the symmetric and antisymmetric stretching modes, respectively.

We note that the Hf−H stretching frequencies for H_2HfO are 1646.4 and 1615.6 cm^{-1} and those for H_2HfS are 1666.8 and 1640.2 cm^{-1} in solid argon.[49] Consistent with this smaller increase in observed frequencies for the sulfide, the computed delocalized dative molecular orbital reaches the H atoms, but does not engulf them as found here for the early actinide metals Th and U. We will continue to pursue this interesting bonding with the lanthanide dihydride sulfides and oxides.

Finally, the terminal $H_2U{-}S$ bond length calculated at the CCSD(T) level of 2.33 Å, is considerably shorter than the 2.74 Å value measured for the solid US material, and the calculated terminal $H_2Th{-}S$ bond lengths, 2.39 and 2.38 Å, are also shorter than the 2.84 Å value measured for the solid ThS.[7]

Reactions in the Matrix. It is interesting to note that the primary reactions of Th and U atoms with H_2S appear to proceed spontaneously since the major H_2ThS and H_2US products *increase* on annealing the solid argon host to 30 K. Calculations of these reaction energies were done at the CCSD(T) level using heats of formation calculated from a set of reaction energies as close to isodesmic as possible and available heats of formation for molecules and atoms (see Supporting Information).[50] The uranium reaction 2 is somewhat less exothermic than the thorium reaction consistent with ThS being about 20 kcal/mol more stable to dissociation than US.[14]

$$^{3}\mathrm{Th} + \mathrm{H_2S} \rightarrow \mathrm{H_2ThS} \qquad \Delta E = -100\ \mathrm{kcal/mol} \tag{1}$$

$$^{5}\mathrm{U} + \mathrm{H_2S} \rightarrow \mathrm{H_2US} \qquad \Delta E = -61\ \mathrm{kcal/mol} \tag{2}$$

The primary products are stable with respect to H_2 elimination (Reactions 3 and 4), although the deposition reactions with excited laser ablated metal atoms do produce some ThS and US on sample deposition.

$$\mathrm{H_2ThS} \rightarrow \mathrm{H_2} + \mathrm{ThS} \qquad \Delta E = 29\ \mathrm{kcal/mol} \tag{3}$$

$$\mathrm{H_2US} \rightarrow \mathrm{H_2} + \mathrm{US} \qquad \Delta E = 9\ \mathrm{kcal/mol} \tag{4}$$

Estimates of the AnS bond energies in the title products are given in reactions 5 and 6. The oxide counterparts are even more exothermic, −197 and −181 kcal/mol, respectively, as expected.

$$\mathrm{S}(^{3}\mathrm{P}) + \mathrm{ThH_2} \rightarrow \mathrm{H_2ThS} \qquad \Delta E = -137\ \mathrm{kcal/mol} \tag{5}$$

$$\mathrm{S}(^{3}\mathrm{P}) + \mathrm{UH_2} \rightarrow \mathrm{H_2US} \qquad \Delta E = -122\ \mathrm{kcal/mol} \tag{6}$$

Secondary reactions of another precursor molecule favored on higher temperature sample annealing also proceed spontaneously, and the exothermic reactions (energies at the CCSD(T) level) given in reactions 7 and 8 provide possible processes.

$$\mathrm{H_2ThS} + \mathrm{H_2S} \rightarrow \mathrm{ThH_2(SH)_2} \qquad \Delta E = -42\ \mathrm{kcal/mol} \tag{7}$$

$$\mathrm{H_2US} + \mathrm{H_2S} \rightarrow \mathrm{UH_2(SH)_2} \qquad \Delta E = -36\ \mathrm{kcal/mol} \tag{8}$$

■ CONCLUSIONS

The reaction of cold Th and U atoms proceeds spontaneously in solid argon at 30 K to form the actinide dihydride sulfide molecules H_2ThS and H_2US, which are identified from matrix infrared spectra using D and S-34 isotopic substitution and matching DFT frequency calculations for the $^{1}A'$ and $^{3}A''$ ground state products. These pyramidal molecules have 71−85 cm^{-1} *higher* actinide-hydrogen stretching frequencies than their actinide dihydride oxide counterparts. The computed molecular orbitals show that S 3p back-bonding to an empty U 6d orbital is delocalized over the H atoms in H_2US whereas owing to the higher electronegativity of O, this does not happen for H_2UO, hence the lower U−H stretching frequencies and longer U−H bonds in the oxide. A similar effect contributes to the Th−H bonds in H_2ThS. As a result there is polarized triple bond character for H_2ThS and H_2US. In these mixed actinide hydride sulfides the An-H bonding is enhanced owing to back-bonding from the softer terminal sulfide ligand.

■ ASSOCIATED CONTENT

Ⓢ Supporting Information

Complete reference 22. Tables of calculated frequencies for secondary reaction products. Frequencies and molecular orbitals for planar subject molecules. Total energies in a.u. Cartesian *x*, *y*, *z* coordinates in Å. Details of the B3LYP NBO analysis. This material is available free of charge via the Internet at http://pubs.acs.org.

■ AUTHOR INFORMATION

Corresponding Author

*E-mail: lsa@virginia.edu (L.A.), dadixon@bama.ua.edu (D.A.D.).

Notes

The authors declare no competing financial interest.

■ ACKNOWLEDGMENTS

We gratefully acknowledge financial support from NSFC Grants (20973126 and 21173158) and STCSM Grant (10PJ1409600) (X.W.) and from DOE Grant DE-SC0001034 and NCSA computing Grant CHE070004N (L.A.) and the DOE BES SISGR program in actinide sciences (D.A.D.). D.A.D. thanks the Robert Ramsay Fund at the University of Alabama and Argonne National Laboratory for partial support. L.A. also thanks M. Kaupp for helpful discussions.

■ REFERENCES

(1) Uranium. In *The Chemistry of the Actinide Elements*, 3rd ed.; Morss, L. R., Edelstein, N. M., J. Fuger.; Springer: Dordrecht, The Netherlands, 2006; Chapter 5, pp 253−698.

(2) Rutkowski, P. X.; Michelini, M. C.; Gibson, J. K. *J. Phys. Chem. A* **2013**, *117*, 451−459.

(3) Liang, B.; Andrews, L.; Li, J.; Bursten, B. E. *J. Am. Chem. Soc.* **2002**, *124*, 6723−6733.

(4) Liang, B.; Hunt, R. D.; Kushto, G. P.; Andrews, L.; Li, J.; Bursten, B. E. *Inorg. Chem.* **2005**, *44*, 2159−2168.

(5) Wang, X. F.; Andrews, L. *Phys. Chem. Chem. Phys.* **2005**, *7*, 3834−3838.

(6) Wang, X. F.; Andrews, L.; Li, J. *Inorg. Chem.* **2006**, *45*, 4157−4166.

(7) Wells, A. F. *Structural Inorganic Chemistry*, 4th ed.; Oxford University Press: New York, 1975.

(8) Liang, B.; Andrews, L.; Ismail, N.; Marsden, C. J. *Inorg. Chem.* **2002**, *41*, 2811−2813.

(9) Liang, B.; Andrews, L. *J. Phys. Chem. A* **2002**, *106*, 4038−4041.

(10) Andrews, L.; Wang, X. F.; Liang, B.; Ruiperez, F.; Infante, I.; Raw, A. D.; Ibers, J. A. *Eur. J. Inorg. Chem.* **2011**, 4457−4463.

(11) Wang, X. F.; Andrews, L.; Marsden, C. *Inorg. Chem.* **2009**, *48*, 6888−6895.

(12) (a) Gaunt, A. J.; Scott, B. L.; Neu, M. P. *Inorg. Chem.* **2006**, *45*, 7401−7407. (b) Ingram, K. I. M.; Tassell, M. J.; Gaunt, A. J.; Kaltsoyannis, N. *Inorg. Chem.* **2008**, *47*, 7824−7833.

(13) (a) Ren, W.; Zi, G.; Fang, D.-C.; Walter, M. D. *J. Am. Chem. Soc.* **2011**, *133*, 13183−13196 and references therein. (b) Brown, J. L.; Fortier, S.; Lewis, R. A.; Wu, G.; Hayton, T. *J. Am. Chem. Soc.* **2014**, *134*, 15468−15475 and references therein.

(14) Pereira, C. C. L.; Marsden, C. J.; Marcalo, J.; Gibson, J. K. *Phys. Chem. Chem. Phys.* **2011**, *13*, 12940−12958.

(15) Dam, H. H.; Reinhoudt, D. N.; Verboom, W. *Chem. Soc. Rev.* **2007**, *36*, 367.

(16) Crabtree, R. H. *The Organometallic Chemistry of the Transition Metals*, 5th ed.; Wiley: New York, 2009.

(17) (a) Andrews, L. *Chem. Soc. Rev.* **2004**, *33*, 123−132. (b) Andrews, L.; Citra, A. *Chem. Rev.* **2002**, *102*, 885−911.

(18) Wang, Q.; Wang, X. F. *J. Phys. Chem. A* **2013**, *117*, 1508−1513.

(19) Becke, A. D. *J. Chem. Phys.* **1993**, *98*, 5648−5653.

(20) Lee, C.; Yang, Y.; Parr, R. G. *Phys. Rev. B.* **1988**, *37*, 785−789.

(21) Perdew, J. P.; Chevary, J. A.; Vosko, S. H.; Jackson, K. A.; Pederson, M. R.; Singh, D. J.; Fiolhais, C. *Phys. Rev. B* **1992**, *46*, 6671−6687.

(22) Frisch, M. J.; Trucks, G. W.; Schlegel, H. B.; Scuseria, G. E.; Robb, M. A.; Cheeseman, J. R.; Scalmani, G.; Barone, V.; Mennucci, B.; Petersson, G. A.; et al. *Gaussian 09*; Gaussian, Inc.: Wallingford, CT, 2009.

(23) Kendall, R. A.; Dunning, T. H., Jr.; Harrison, R. J. *J. Chem. Phys.* **1994**, *96*, 6796−6806.

(24) Dunning, T. H., Jr.; Peterson, K. A.; Wilson, A. K. *J. Chem. Phys.* **2001**, *114*, 9244−9253.

(25) Vent-Schmidt, T.; Hunt, R. D.; Andrews, L.; Riedel, S. *Chem. Commun.* **2013**, *49*, 3863−3865.

(26) Lyon, J. T.; Andrews, L.; Ismail, N.; Malmqvist, P.-A.; Roos, B. O.; Yang, T.; Bursten, B. E. *Inorg. Chem.* **2007**, *46*, 4917−4925.

(27) Wang, X. F.; Andrews, L.; Marsden, C. J. *Chem.—Eur. J.* **2008**, *14*, 9192−9201.

(28) Bartlett, R. J.; Musial, M. *Rev. Mod. Phys.* **2007**, *79*, 291−352.

(29) (a) Deegan, M. J. O.; Knowles, P. J. *Chem. Phys. Lett.* **1994**, *227*, 321−327. (b) Knowles, P. J.; Hampel, C.; Werner, H. J. *J. Chem. Phys.* **1993**, *99*, 5219−5227. (c) Rittby, M.; Bartlett, R. J. *J. Phys. Chem.* **1988**, *92*, 3033−3036.

(30) Jackson, V. E.; Craciun, R.; Dixon, D. A.; Peterson, K. A.; de Jong, W. A. *J. Phys. Chem. A* **2008**, *112*, 4095−4099.

(31) *MOLPRO*, version 2010.1, a package of ab initio programs; Knowles, P. J.; Manby, F. R.; Schütz, M.; Celani, P.; Knizia, G.; Korona, T.; Lindh, R.; Mitrushenkov, A.; Rauhut, G.; Adler, T. B.; et al.; see http://www.molpro.net

(32) (a) Hunt, R. D.; Andrews, L. *J. Chem. Phys.* **1993**, *98*, 3690−3696. (b) Hunt, R. D.; Yustein, J. T.; Andrews, L. *J. Chem. Phys.* **1993**, *98*, 6070−6074.

(33) Souter, P. F.; Kushto, G. P.; Andrews, L.; Neurock, M. *J. Phys. Chem. A* **1997**, *101*, 1287−1291.

(34) Souter, P. F.; Kushto, G. P.; Andrews, L.; Neurock, M. *J. Am. Chem. Soc.* **1997**, *119*, 1682.

(35) Raab, J.; Lindh, R. H.; Wang, X. F.; Andrews, L.; Gagliardi, L. *J. Phys. Chem. A* **2007**, *111*, 6383−6387.

(36) Jacox, M. E. *Chem. Phys.* **1994**, *189*, 149−170.

(37) Zhou, M. F.; Andrews, L.; Li, J.; Bursten, B. E. *J. Am. Chem. Soc.* **1999**, *121*, 9712−9721.

(38) Andrews, L.; Liang, B.; Li, J.; Bursten, B. E. *J. Am. Chem. Soc.* **2003**, *125*, 3126−3139.

(39) Wang, X. F.; Andrews, L.; Gagliardi, L. *J. Phys. Chem. A* **2008**, *112*, 1754−1761.

(40) Wang, X. F.; Andrews, L.; Marsden, C. J. *Chem.—Eur. J.* **2007**, *13*, 5601−5606.

(41) (a) Weinhold, F. In *Encyclopedia of Computational Chemistry*; P. v. R. Schleyer, Ed.; John Wiley & Sons: Chichester, U.K., 1998; Vol. 3, pp 1792−1811; (b) Weinhold, F.; Landis, C. R. *Valency and Bonding: A Natural Bond Orbital Donor-Acceptor Perspective*; University Press: Cambridge, U.K., 2003. (c) Reed, A. E.; Weinstock, R. B.; Weinhold, F. *J. Chem. Phys.* **1985**, *83*, 735−746. (d) Reed, A. E.; Curtiss, L. A.; Weinhold, F. *Chem. Rev.* **1988**, *88*, 899−926.

(42) Gong, Y.; Wang, X. F.; Andrews, L.; Schlöder, T.; Riedel, S. *Inorg.Chem.* **2012**, *51*, 6983−6991.

(43) Andrews, L.; Cho, H.-G. *J. Phys. Chem. A* **2005**, *109*, 6796−6798.

(44) Roos, B. O.; Lindh, R. H.; Cho, H.-G.; Andrews, L. J. *J. Phys. Chem. A* **2007**, *111*, 6420−6424.

(45) Andrews, L.; Wang, X. F.; Lindh, R.; Roos, B. O.; Marsden, C. J. *Angew. Chem.* **2008**, *47*, 5446−5450; *Angew. Chem., Int. Ed.* **2008**, *47*, 5366−5370.

(46) Andrews, L.; Gong, Y.; Liang, B.; Jackson, V. E.; Flamerich, R.; Li, S.; Dixon, D. A. *J. Phys. Chem. A* **2011**, *115*, 14407−14416.

(47) Wang, X. F.; Andrews, L. *Dalton Trans.* **2009**, 9260−9265.

(48) te Velde, G.; Bickelhaupt, F. M.; van Gisbergen, S. J. A.; Fonseca, C.; Guerra, E. J.; Baerends, J. G.; Snijders, T.; Ziegler, T. *J. Comput. Chem.* **2001**, *22*, 931−967.

(49) (a) Zhou, M. F.; Zhang, L. N.; Dong, J.; Qin, Q. Z. *J. Am. Chem. Soc.* **2000**, *122*, 10680−10688. (b) Wang, X. F. unpublished results, 2013.

(50) (a) Konigs, R. J. M.; Benes, O. J. *J. Phys. Chem. Ref. Data* **2010**, *39*, 043102. (b) Konigs, R. J. M.; Morss, L. R.; Fuger, J. In *The Chemistry of the Actinide and Transactinide Elements*, 3rd ed.; Morss, L. R., Edelstein, N. M., Fuger, J., Eds.; Springer: Dordrecht, The Netherlands, 2006; Chapter 19, Vol. 4, pp 2113−2224. (c) Cox, J. D.; Wagman, D. D.; Medvedev, V. A. *CODATA Key Values for Thermodynamics*; Hemisphere: New York, 1989. (d) Chase, M. W., Jr. NIST-JANAF Thermochemical Tables, 4th ed.; *J. Phys. Chem. Ref. Data, Monogr. 9*; American Institute of Physics: Woodbury, NY, 1998; Suppl. 1.